Naval Medical Research Institute
Bethesda, MD 20814-5055
NMRI 88-23
November 1988

(2)

ROBUST SPATIAL CALIBRATION OF A PLANAR POSITRON CAMERA

PAUL K. WEATHERSBY,
SHALINI S. SURVANSHI,
and PAUL MEYER

Naval Medical Research
and Development Command
Bethesda, Maryland 20814-5044

Department of the Navy
Naval Medical Command
Washington, D.C. 20372-5210

UNCLASSIFIED
SECURITY CLASSIFICATION OF THIS PAGE

REPORT DOCUMENTATION PAGE

1a REPORT SECURITY CLASSIFICATION UNCLASSIFIED	1b RESTRICTIVE MARKINGS
2a SECURITY CLASSIFICATION AUTHORITY	3 DISTRIBUTION/AVAILABILITY OF REPORT Approved for public release; distribution is unlimited
2b DECLASSIFICATION/DOWNGRADING SCHEDULE	
4 PERFORMING ORGANIZATION REPORT NUMBER(S) NMRI 88-23	5 MONITORING ORGANIZATION REPORT NUMBER(S)
6a NAME OF PERFORMING ORGANIZATION Naval Medical Research Institute 6b OFFICE SYMBOL (If applicable)	7a NAME OF MONITORING ORGANIZATION Naval Medical Command
6c ADDRESS (City, State, and ZIP Code) Bethesda, Maryland 20814-5055	7b ADDRESS (City, State, and ZIP Code) Department of the Navy Washington, D. C. 20372-5120
8a NAME OF FUNDING/SPONSORING ORGANIZATION Naval Medical Research & Development Command 8b OFFICE SYMBOL (If applicable)	9 PROCUREMENT INSTRUMENT IDENTIFICATION NUMBER
8c ADDRESS (City, State, and ZIP Code) Bethesda, Maryland 20814-5044	10 SOURCE OF FUNDING NUMBERS PROGRAM ELEMENT NO. 63713N; PROJECT NO. M0099; TASK NO. .01A; WORK UNIT ACCESSION NO. DN177792

11 TITLE (Include Security Classification)

ROBUST SPATIAL CALIBRATION OF A PLANAR POSITRON CAMERA

12 PERSONAL AUTHOR(S)
Paul K. Weathersby+, Shalini S. Survanshi, and Paul Meyer*

13a TYPE OF REPORT	13b TIME COVERED	14 DATE OF REPORT (Year, Month, Day)	15 PAGE COUNT
Final	FROM 10/85 TO 09/87	October 1988	27

16 SUPPLEMENTARY NOTATION

+Naval Submarine Medical Research Laboratory; Groton, CT 06349
*Lawrence Livermore National Laboratory; Livermore, CA 94550

17 COSATI CODES			18 SUBJECT TERMS (Continue on reverse if necessary and identify by block number)
FIELD	GROUP	SUB-GROUP	Positron, instrumentation, image, mathematical model, error distribution

19 ABSTRACT (Continue on reverse if necessary and identify by block number)

The planar positron camera is a three-dimensional imaging device with two parallel and planar large crystal detectors. The spatial calibration problem is to define the relation between the raw digitized detector output to a physical coordinate system in the imaged space. In a calibration procedure, a positron point source is placed in a series of known emission locations during data acquisition. Data is then fit to a mathematical model to estimate spatial offsets and gains in the detector. Fitting procedures require some assumptions about error distribution, and the assumption of normally distributed error used in least-squares estimation does not appear suitable for these detectors. In simulated data sets, alternative non-normal distributions ("robust estimators") allowed successful recovery of camera spatial parameters even with a few hundred total detected positron emissions. With experimental data, the robust procedures avoided the unreasonable camera performance parameters estimated by least-squares.

20 DISTRIBUTION/AVAILABILITY OF ABSTRACT	21 ABSTRACT SECURITY CLASSIFICATION
☒ UNCLASSIFIED/UNLIMITED ☐ SAME AS RPT. ☐ DTIC USERS	
22a NAME OF RESPONSIBLE INDIVIDUAL Mrs. Phyllis Blum, Information Services Div.	22b TELEPHONE (Include Area Code) (202) 295-2188
	22c OFFICE SYMBOL ISD/RSD/NMRI

DD FORM 1473, 84 MAR 83 APR edition may be used until exhausted. All other editions are obsolete.

SECURITY CLASSIFICATION OF THIS PAGE

UNCLASSIFIED

TABLE OF CONTENTS

LIST OF FIGURES

LIST OF TABLES

ACKNOWLEDGEMENTS

This study was supported by the Naval Medical Research and Development Command, Work Unit No. M0099.01A.0005. The editorial services of D. Temple, S. Cecire, and J. Gaines are gratefully acknowledged. The views, opinions, and/or assertions herein are those of the authors and should not be construed as official or reflecting the views, policy, or decision of the United States Navy or the naval service at large.

I. INTRODUCTION

Substantial current and potential medical interest exists in use of tracers containing positron emitting isotopes. The isotopes ^{11}C, ^{13}N, and ^{15}O offer the ability to tag biochemical compounds without altering the primary covalent structure of the molecule, and the short (2-20 min) half-lives reduce the patient radiation exposure after completion of the tracer study. In a few centers, these isotopes are being applied to measure local blood flow, volumes, pH, and metabolic activity level (1,2,3,4). Presently, exploitation of the many potential clinical applications lags far behind single photon technology because of substantial costs of isotope production and data acquisition. Progress has also been slow in obtaining analysis techniques that fulfill the quantitative potential of positron imaging.

This paper addresses one problem in quantitation of positron images: spatial calibration of one type of detector. In the calibration described, we encountered unsatisfactory parameter estimates from normal treatment of errors because the errors did not follow a Gaussian distribution. Section II describes the context of the problem. Section III reviews the process of acquiring calibration data and of simulating the same process. Section IV presents a mathematical model of the physical detection process and identifies the camera performance parameters that must be estimated from the data. Section V discusses several possible formulations of how noise corrupts the data. Use of maximum likelihood to fit data to the models and estimate camera performance is also presented in this section. Section VI presents the results of camera performance estimates for several simulated and actual sets of data.

II. PROBLEM CONTEXT

Most recent positron work has focused on specialized detectors designed

with one or more coplanar rings of many individual gamma detectors (3,4). These ring devices produce a two-dimensional image of isotope distribution within the detector plane. However, the earliest positron emission work used a pair of large area planar detectors (5). They are versatile in being able to fit around a large or irregular volume, and they are efficient in covering a larger solid angle than ring designs. Modern versions sometimes add the cost of rotating the detectors around the patient to increase sampling of the possible emission angles (6).

In these devices, two position sensitive gamma detectors (e.g., Anger cameras) are operated in coincidence (4,5,7,8). The detectors are set to record the gamma arrival locations only when each has simultaneously processed a 511 KeV positron annihilation photon. The clinical data set consists of a large number of photon location lines (typically 10^4 to 10^7) defined by the intersection location of the gammas on each of the 2 camera faces. An analytical challenge exists to resolve this set of lines into a full three-dimensional map of the positron annihilation density, i.e., the tracer distribution within the patient. However, a more primitive quantitative problem concerns us here: that of understanding the position signal of each single event.

The raw spatial information of the devices is a set of digital position signals that are subject to many analog processing steps (1,7,8). Direct knowledge of the spatial events is limited by the random direction of each gamma emission event. Furthermore, the originally 180 degree opposed gamma trajectories may have been changed by scattering processes within the patient or the detector, and some of the events may be random coincidences of gammas from different events (1,2,3,5). Thus it is necessary to calibrate the spatial performance of the detectors. Calibration here is defined as the

process of extracting detector spatial performance parameters from a set of positron annhilation data. Calibration is necessary if the data is to be used to extract spatial features of the tracer distribution (e.g., lengths or volumes). Spatial calibration is especially important if one desires translocation of the data to another coordinate system, such as an X-ray image of the same patient, or if one intends to use a three-dimensional reconstruction method that includes specific features of a given detector (9,10). Finally, a method was desired that could use a small number of recorded events to minimize patient radiation dose. All these requirements were applied in a recent study where we desired quantitative ^{13}N measurements in healthy human subjects (11).

Spatial calibration has not received much attention in the literature. Ring detectors operate by coincidence of separate discrete detectors so the location of the reported emission line is nearly known from the external detector locations (4). Large area detectors are most often used in single photon imaging. Standard set-up procedures concentrate on assuring a uniform response across the camera face ("flood correction") (2,12). Some correction procedures are available for other point-to-point distortions (13,14), but most interpretations compare features within an image rather than use an external or calibrated size scale. When a spatial calibration is desired for a single photon camera, a distant point source can be imaged through a lead-shielding pattern of known dimensions. The technique is not applicable to positron use of the camera because of the inherent three-dimensional nature of the images.

III. DATA

Spatially calibrating the positron detector consists of placing a single positron point source (typically ^{22}Na) at a series of known locations and

recording position-related signals of the annihilation gamma ray events and the emission location itself. Our detector is a pair of Anger cameras operated in coincidence that output signals based on weighting the individual phototubes (15). The digitized signals (an X and Y coordinate for each Anger camera head) or their simulated equivalent are the raw data for each positron event. In a typical situation, 100-300 photon pairs were recorded for each point source location.

Experimental (and simulated) geometry had two 20 cm radius NaI detectors aligned with a separation of 46 cm. Raw X and Y positions for each event satisfying energy and coincidence windows were logged in 0-127 A to D converter (ADC) units. For the simulated experiments, a spherically uniform random direction was first obtained. If both rays of the emission intersected the camera circles, the intersection coordinates were calculated. To each intersection coordinate an error was added by generating a Gaussian (normal) error with zero mean and a specified standard deviation (σ) and random direction. Thus the emission was simulated as error-free; detection error was limited to the camera faces. In one series of simulations, an additional error source was used: a specified fraction (f) of the total events was produced by generating a uniform random variable for each coordinate.

Specific conditions for some simulated and actual data are presented in Table 1. Data sets A and B were obtained by simulation with and without the uniform error. In all simulations, offsets were zero and the camera ADC gains were set to 128 ADC units/40 cm = 3.2 unit/cm. An extensive calibration experiment produced data set C. Set D is from a source held at four prominent points on the body of a human subject during an actual physiology experiment (11). Recorded activity was deliberately kept at a minimum.

IV. PHYSICAL MODEL

A mathematical description of the process must be used to relate data to aspects of the detector. The physics of the detected event depends upon detector performance under study. We chose to seek the spatial gain of each camera amplifier as well as offsets between camera center and midpoint of digitized output. Each event is treated by simple backprojection as shown in Fig. 1.

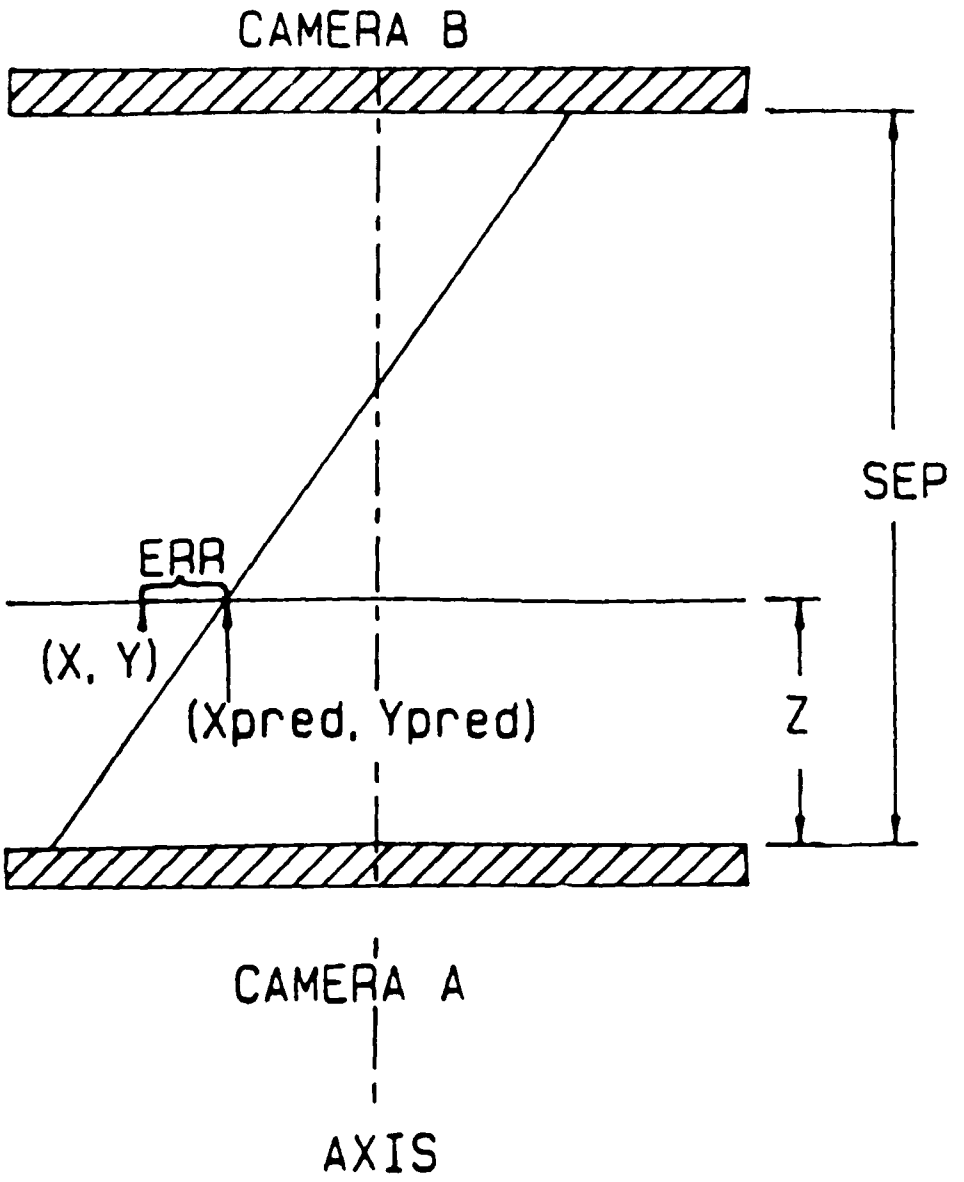

Fig. 1. Geometry of backprojection and error definition.

$$Xpred_i = (Z_i/SEP) \cdot \left[(XbRaw_i - XofsB - 64)/GainB\right] + (1.0 - Z_i/SEP) \cdot \left[(XaRaw_i - XofsA - 64)/GainA\right] \quad [1]$$

$$Ypred_i = (Z_i/SEP) \cdot \left[(YbRaw_i - YofsB - 64)/GainB\right] + (1.0 - Z_i/SEP) \cdot \left[(YaRaw_i - YofsA - 64)/GainA\right] \quad [2]$$

The symbols in the equations are identified as follows:

Symbol	Description	Unit	Measured/Estimated
SEP	camera face separation	cm	measured
Z_i	distance of point source i above (bottom) camera A	cm	measured
$XaRaw_i$	raw X coordinate of event from source i on camera A	ADC unit	measured
$XbRaw_i$	same, on camera B	ADC unit	measured
$YaRaw_i$	raw Y coordinate of event from source i on camera A	ADC unit	measured
$YbRaw_i$	same, on camera B	ADC unit	measured
XofsA	offset between camera A physical center and ADC center in X direction	ADC unit	estimated
XofsB	same, on camera B	ADC unit	estimated
YofsA	offset between camera A physical center and ADC center in Y direction	ADC unit	estimated
YofsB	same, on camera B	ADC unit	estimated
Gain A	distance amplification factor on camera A	ADC unit per cm	estimated
Gain B	same, on camera B	ADC unit per cm	estimated
$Xpred_i$	predicted distance of source i in X direction from camera axis at plane Z_i	cm	(estimated)
$Ypred_i$	same in Y direction	cm	(estimated)

This model assumes that X and Y gains are the same in a given camera (no deviation from circularity), but that the 2 cameras may have a different gain.

Subtraction of 64 translates the coordinate system to the center of the 0-127 output range. With enough recorded events from enough point sources many more features of the detection process can be modelled for calibration, but these few have gained the major attention in our experiments. A data set consists of hundreds of raw events: X_i, Y_i, Z_i are the externally measured location of the point sources from the center of camera A (presumed to be known precisely). The modelling then attempts to use these data to estimate the (presumed unknown) positron camera parameters: 4 offsets and 2 gains. In experiments on human subjects another 2 parameters are estimated to align the axes of the positron camera with the center-line of a flat-plate X-ray image of the subjects obtained later. X,Y data in that case are measured from the x-ray after correction for fan-beam expansion. Note that X,Y,Z must be known for each emission, so only a single point source can be in the camera field.

V. STATISTICAL MODEL

For any fit, the values of the parameters to be estimated are adjusted until the "error" between model calculated and actually measured data is minimized. First, the "error" must be defined. We take the error to be a single radial deviation (in other physical models it may be more appropriate to treat X and Y direction errors separately).

$$ERR_i = \left[(X_i - Xpred_i)^2 + (Y_i - Ypred_i)^2 \right]^{\frac{1}{2}} \qquad [3]$$

For continuous variables the widely used principle of least squares minimizes the error in a root mean square manner. Least-squares, however, assumes that the data will fall around the model predictions according to a normal Gaussian curve. If there is reason to expect non-Gaussian behavior, then another treatment of error may be preferred. Such is the case with position-sensitive gamma detectors where the distribution of events tends to have a well defined peak, but fails to fall off as rapidly as $\exp(-x^2)$ away from the mean. An

example from our work is shown in Fig. 2; other examples are Fig. 3 of Cook et al. (16), and Fig. 7 of Perez-Mendez et al. (17). The peak is sharp, but off-peak events are not as rare as a Gaussian distribution. In fact, slight but measurable activity seems to emanate from all locations: a sort of spatially uniform noise. Such large deviations from the original point can arise from known processes, such as Compton scattering of the photons, and accidental coincidence of unpaired photons (7). The usual treatment of these distributions is to report peak width at half of the maximum (FWHM) as a measure of resolution. Such an approach does not directly lead to a statistical evaluation.

Since least-squares estimates weigh deviant points heavily, estimates can be highly biased if some outlying points exist in the data sets. To avoid or minimize such biases, techniques of "robust estimation" have been developed (18,19). Robust estimators generally assign less weight to data points far from the most probable location. The "M-estimator" of Huber (18) is one well developed approach; in general one can use an error distribution that corresponds to the processes under consideration.

A formal procedure is needed to estimate parameters for a given error distribution. By the general principle of maximum likelihood, the estimation procedure adjusts parameters to maximize the total probability of obtaining the data set - the likelihood function (20). Assuming all recorded events to be independent, this is equivalent to maximizing the product of the probability of all data points (the $p(ERR_j)$). Since all probabilities are less than 1, the sum of the logs of the probability (i.e., log likelihood, LL) are more conveni

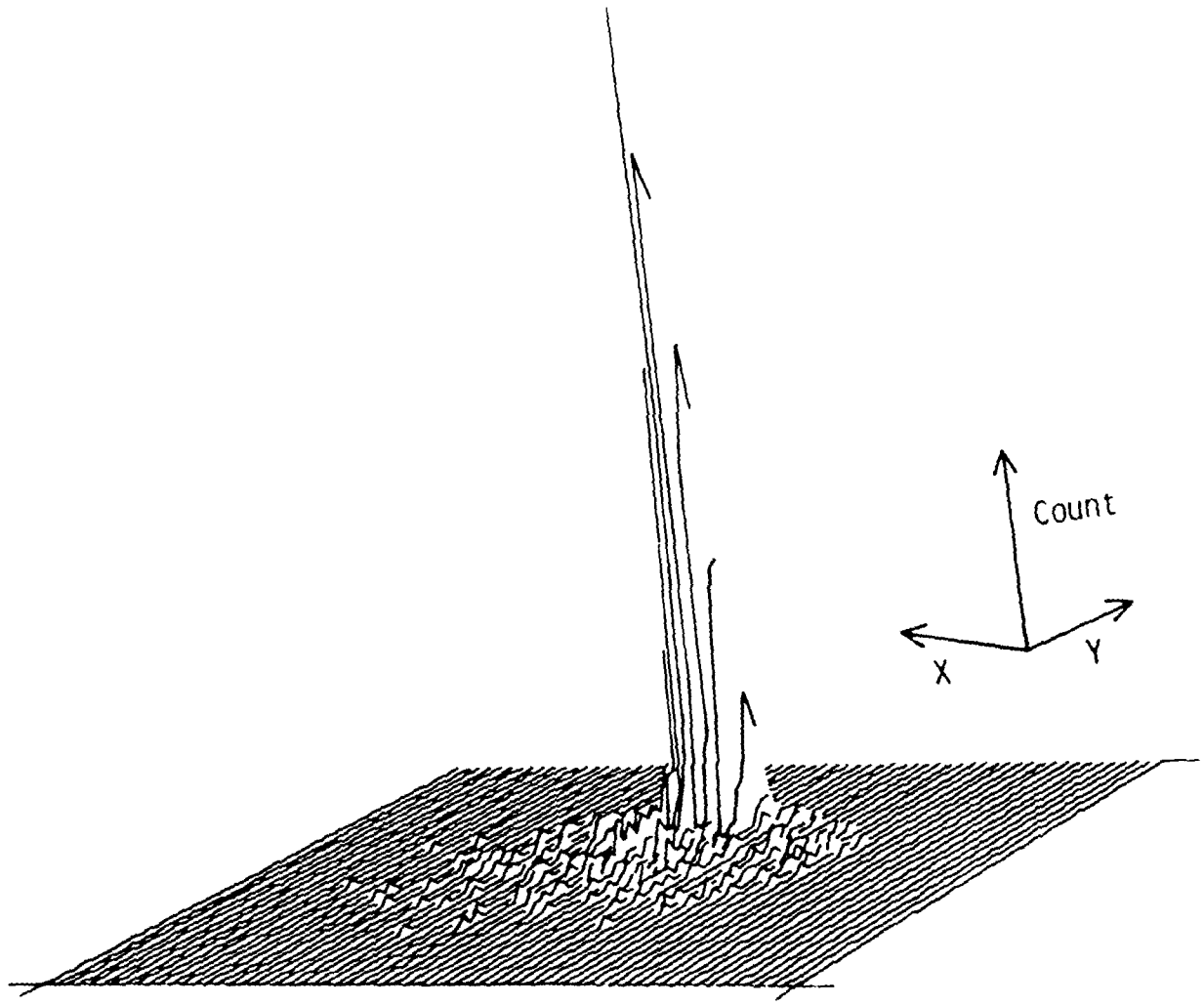

Fig. 2. Distribution of counts from a single point source backprojected into plane of emission. Note the significant number of counts far from the peak and covering most of the camera cross sectional area (camera diameter is about 3/4 of X and Y display width). For this image, 1792 counts were collected from a ^{22}Na source 23 cm above camera A and 1.4 cm from the camera center in the Y direction. Raw ADC units were used for backprojection.

$$LL = \sum_{j=1}^{data} \ln\left(p(ERR_j)\right) \qquad [4]$$

LL is then a measure of goodness-of-fit between the overall model and the data set. Increases in LL can be used to choose the better fitting model. Model comparison can be formally constructed with a chi-square test statistic (20). Maximum likelihood has previously been used in performance evaluation of single scintillation cameras (21) and is now being used in the image reconstruction problem (9,10,22).

Three models of p(ERR) were examined. First is the normal distribution:

$$p(ERR) = (2\pi\sigma^2)^{-\frac{1}{2}} \exp\left(-ERR^2/2\sigma^2\right) \qquad [5]$$

The only statistical parameter in this distribution is σ, the standard deviation of spatial error in the focal plane. The other parameter in the usual expression for the normal distribution (i.e., the mean) is defined by the physical model described above. Substitution of Eqn. (5) into the likelihood criterion, Eqn. (4), can be shown to lead to the usual least-squares criterion of minimizing ERR^2 summed over the data. Next is the more robust M distribution suggested by Huber (18):

$$\begin{aligned} p(ERR) &= (K\sigma)^{-1} \exp\left(-ERR^2/2\sigma^2\right) && \text{for } ERR < \textcircled{a}\cdot\sigma \\ &= (K\sigma)^{-1} \exp\left(-\textcircled{a}\cdot ERR/\sigma + \textcircled{a}^2/2\right) && \text{for } ERR > \textcircled{a}\cdot\sigma \end{aligned}$$

$$\text{where} \quad K = 2\left(\exp(-\textcircled{a}^2/2)\right)/a + \int_0^{\textcircled{a}} \exp(-x^2/2)\,dx \qquad [6]$$

Here ⓐ is an adjustable parameter which sets the demarcation between a normal tail and a slower fall-off. Some desirable statistical properties occur when ⓐ = 1.5 (19). We used a fixed at 1.5 and also attempted to estimate it. The third model has a uniform distribution superimposed on a normal distribution:

$$p(ERR) = f/W + (1-f)(2\pi\sigma^2)^{-\frac{1}{2}} \quad \exp(-ERR^2/2\sigma^2) \qquad [7]$$

Here f is the fraction of the total detected events that may hit anywhere on the camera face (whose diameter is W).

All 3 distributions are plotted in Fig. 3. As expected, all have a similar "sharpness" near the middle, with the sharpness controlled by parameter σ in all models. The normal falls off quickly: exponentially with distance squared. The Huber M falls initially as fast and then as exp(-x) after $(ERR/\sigma) > (a)$. Thus a perceptible probability of an event is expected out to a distance of nearly 5 σ instead of less than 3 σ with the normal. The normal plus uniform falls rapidly at first, then merges with a single uniform expected level of activity. The most appropriate model is determined by known or assumed features of the data.

All 3 models were applied to the data sets described above and the results are presented in the following tables. For fitting we used a Marquart non-linear algorithm (23), modified to perform maximum likelihood estimates (24). The program estimates 1 SE error limits on the estimated parameters by inverting the Fisher information matrix. These error estimates are expected to be only approximately correct (20).

RESULTS

The first simulated data set, A, was generated with only normal error on each camera face and no uniform noise. All 4 entries in Table 2 show the best-fit parameters to be close to their nominal values. Estimated offsets are all within 1 ADC unit, which is the degree of ambiguity in the simulation procedure used. Camera gains were recovered within a few percent of their actual values. The standard deviations were all slightly underestimated for reasons that are not understood. The first entry for Huber's M-distribution is a significantly worse fit to the 1200-event data file. The decrease of

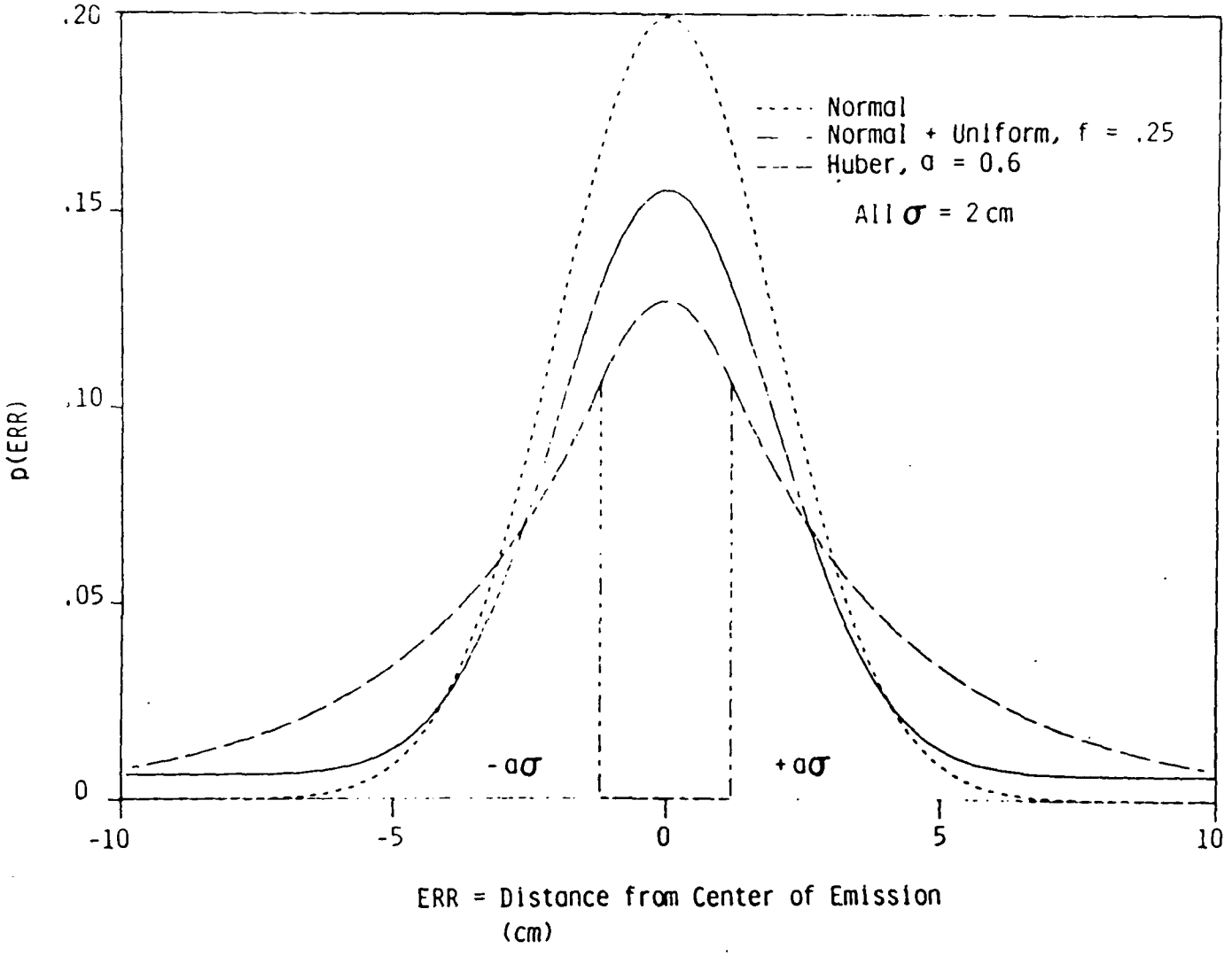

Fig. 3. Three alternative error distributions. In all cases σ is 2 cm.

maximum LL from -1715 to -1733 is actually a substantial loss in goodness-of-fit. (In order to justify the inclusion of an additional parameter in a general model, an increase in LL of about 1.9 is required to conclude significant improvement with 95% confidence.) (20). When that parameter was estimated by the data, the best fit was (a) = 2.9. This value leaves the error distribution essentially normal, since only a few events would lie outside (a). The last line in Table 1 reflects our attempts to estimate parameter f. No finite value of f, the uniformly distributed fraction, achieved a better fit to the data than f = 0. The values of LL for 3 of the 4 models are essentially equal and therefore describe the data equally well.

Other simulations with normal error distributions led to several conclusions. First, increase of the number of recorded events per source location to 1000 led to no real improvement in estimation. Second, simulated performance degradation (σ doubled) sometimes led to unrealistic offsets. Third, the number of source locations could be important: the worst problems were with 3 or 4 locations that were close to collinear in the detection volume.

Simulated data set B had a fraction of 0.14 of the total events recorded at uniformly random positions on the camera face to simulate spatial "white noise". Other aspects of the simulation were as Set A. Results listed in Table 3 show that a normal distribution cannot fit the data well, forcing large and misleading offsets (from -22 to +65 ADC units), camera gains, and standard deviation. Huber's M-estimator with the recommended (a) = 1.5 is better both as a fit to the data (much greater LL) and in recovering starting values of the camera parameters. Allowing (a) to be estimated produces an even better fit with the estimated gains slightly higher than simulated. The low

value of ⓐ (0.40) means that only a small fraction of the distribution was chosen to have a normal shape. The final entry in Table 3 shows a successful recovery of camera parameters with the normal + uniform distribution. The progressive increase in LL going down Table 3 shows striking improvement in fit with each model.

Similar analyses performed on real data are summarized in Table 4. This data set was constructed of 1,596 gamma events from 15 point source locations within the camera field of view. The first line in Table 4 gives estimated offsets that were within a few ADC units of perfect centering, but the camera gains were larger than seemed reasonable when examining the actual distribution of events on the camera faces. The standard deviation of over 5 cm also seems too large because this corresponds to a FWHM of 7 cm, if the distribution is indeed Gaussian. Simple backprojections showed much better resolution expressed as FWHM. The second line in the table is the result of applying Huber's robust estimator and the fit has a much better LL. The offsets, gains, and standard deviation are all smaller. If Huber's parameter ⓐ is estimated, an even better description is obtained. The best result is the final table entry indicating that about 14% of the events do not arise from the nearby vicinity of the point sources themselves. Such a fraction is within the range expected in some positron detectors (3,6). The modest offsets and the magnitude of the gains are both supported by examination of raw images on the camera faces.

The final data set, D, (Table 5) is from the biological experiments (11) in which we mapped the positron records onto a coordinate system defined by a flat-plate X-ray of the same subject. For these data, a slightly different model was used. The ADC to camera center offsets were fixed at the values shown in Table 4 because the acquisition system was not "re-tuned" between the

two experiments. However, a coordinate pair XX, XY was included to translate the camera center to the X-ray center. Statistical models remained the same. As seen in Table 5, the normal distribution alone was not a good representation of the data. Huber's distribution produced a better fit, but by maximum likelihood the best was a combination of normal and uniform. The estimated uniform fraction was nearly the same as for data set C.

VI. DISCUSSION

The robust estimation procedures presented here are most useful when important features of a distribution are unknown. As discussed in texts on robust estimation, a reassuring feature of this work was the similar positron camera calibration parameters found with different non-normal distributions. This implies that the needed parameters are likely to be nearly correct even if we are uncertain of the actual error distribution. What makes the distribution markedly non-Gaussian? First, many photons are scattered to different directions while maintaining enough energy to still be accepted by the nominal 511 KeV discriminator. The spatial distribution of scattered photons depends strongly on the emitter and scatterer density in 3 dimensions, and will vary with movement of any solid object in the field. Small angle scattering is likely to appear as a broader peak in the distribution, while large angle events will provide a more diffuse noise. Random coincidences are more of a problem in high activity situations when the single photon arrival rate at each camera approaches the time resolution of the discrimination circuits. The rate is low in the calibration procedure described so only a small fraction of the recorded events should arise from this source. Those that are recorded would be expected to be spatially random.

The low count rate used in this procedure offered other advantages in our biological experiments (11). Radiation dose to the human subject was

minimized, and camera performance data could be recorded within a few minutes of the desired physiological kinetic data. Even the error distribution information (parameters σ and f) can be directly used in a specific maximum likelihood image reconstruction procedure (25).

The necessity of so detailed an analysis in routine clinical use is uncertain. Most clinical work produces a raw image and many quantitative shortcomings are accepted. Certainly some applications, like length or volume measurements, would require some spatial calibration, but the specifics of the model need to be tailored to the specific device and the intended application. Our procedure has revealed a number of device features not previously apparent, such as non-equal camera gains. Robust procedures should be considered in other applications, since serious bias in parameter estimates can result from incorrect error distributions even when other problems (e.g., Poisson counting errors) are overcome.

REFERENCES

1. Brownell, G.L., Correia, J.A., and Zamenhof, R.G., "Positron instrumentation." Recent Advances in Nuclear Medicine, Vol. 5, pp. 1-49, 1978.

2. Muehllehner, G. and Colsher, J.G., "Instrumentation." In: Computed Emission Tomography. Ell, P.J. and Holman, B.L., editors. Oxford: Oxford University Press, pp. 3, 1982.

3. Budinger, T.F., Gullberg, G.T., and Huesman, R.H. "Emission computer tomography." In: Image Reconstruction from Projections. Herman, G.T., editor. Berlin: Springer-Verlag, pp, 147-246, 1979.

4. Hoffman, E.J. and Phelps, M.E., "Positron emission tomography: principles and quantitation." In: Positron Emission Tomography and Autoradiography: Principles and Application to the Brain and Heart. Phelps, M.E., Mazziotta, J.C. and Schelbert, H.R., editors. New York: Raven Press, pp. 237-286, 1986.

5. Brownell, G.L., "Theory of radioisotope scanning." International Journal of Applied Radiation and Isotopes, Vol. 3, pp. 181-192, 1958.

6. Paans, A.M.J., Vaalburg, W., and Woldring, M.G., "A rotating double-headed positron camera." Journal of Nuclear Medicine, Vol. 26, pp. 1466-1471, 1985.

7. Kenny, P.J., "Spatial resolution and count rate capacity of a positron camera: some experimental and theoretical considerations." International Journal of Applied Radiation and Isotopes, Vol. 22, pp. 21-28, 1971.

8. Muehllehner, G., Buchin, M.P., and Dudek., J.H. "Performance parameters of a positron imaging camera." IEEE Transactions on Nuclear Science, Vol. NS-23, pp. 528-537, 1976.

9. Llacer, J. and Meng, J.D. "Matrix-based image reconstruction methods for tomography." IEEE Transactions on Nuclear Science, Vol. NS-32, pp. 855-864, 1985.

10. Floyd, Jr., C.E., Jaszczak, R.J., and Coleman, R.E., "Inverse Monte Carlo: a unified reconstruction algorithm for SPECT." IEEE Transactions on Nuclear Science, Vol. NS-32, pp. 779-785, 1985.

11. Weathersby, P.K., Meyer, P., Flynn, E.T., Homer, L.D., and Survanshi, S.S., "Nitrogen gas exchange in the human knee." Journal of Applied Physiology, Vol. 61, pp. 1534-1545, 1986.

12. Paans, A.M.J., E.J. de Graaf, J. Welleweerd, W. Vaalburg, and M.G. Woldring, "Performance parameters of a longitudinal tomographic positron imaging system." Nuclear Instruments and Methods, Vol. 192:491-500, 1982.

13. Muehllehner, G., Colsher, J.G., and Stoub, E.W., "Correction for field nonuniformity in scintillation cameras through removal of spatial distortion." Journal of Nuclear Medicine, Vol. 21, pp. 771-776, 1980.

14. Wicks, R. and Blau, M. "Effect of spatial distortion of Anger camera field-uniformity correction: concise communication." Journal of Nuclear Medicine, Vol. 20, pp. 252-254, 1979.

15. Behrin, E., Positron/scintillation camera data acquisition and display system, Lawrence Livermore Laboratory, UCRL-51288, 1972.

16. Cook, W.R., Finger, M., and Prince, T., "A thick Anger camera for gamma-ray astronomy." IEEE Transactions on Nuclear Science, Vol. NS-32, pp. 129-133, 1985.

17. Perez-mendez, V., Lim, C.B., Ortendahl, D., Semper, R., Cheng, A., Chu, D., Hattner, R., Kaufman, L., and Price, D.C., "Two detector MWPC positron camera with honeycomb lead converters for medical imaging: performance and developments." Nuclear Instruments and Methods, Vol. 156, pp. 33-40, 1978.

18. Huber, P.J., "Robust statistical procedures". Philadelphia: Society for Industrial and Applied Mathematics, 1977.

19. Launer R.L. and C.N. In: Robustness in statistics, Wilkinson, G.N., editor. New York: Academic Press, 1979.

20. Kendall, M. and Stuart, A. The advanced theory of statistics, Fourth Edition, Vol. 2. New York: Macmillan, 1979.

21. Gray, R.M. and Macovski, A., "Maximum a posteriori estimation of position inscintillation cameras." IEEE Transactions on Nuclear Science, Vol. NS-23, pp. 849-852, 1976.

22. Shepp, L.A. and Vard, Y. "Maximum likelihood reconstruction for emission tomography." IEEE Transactions on Medicine Imaging, Vol. MI-1, pp. 113-122, 1982.

23. Marquardt, D.W., "An algorithm for least-squares estimation of nonlinear parameters." Journal of Society of Industrial Applied Math, Vol.11, pp. 431-441, 1963.

24. Bailey, R.C. and Homer, L.D., "An analogy permitting maximum likelihood estimation by a simple modification of general least squares algorithms." Naval Medical Research Institute Technical Report No. 77-55, 1977, (NTIS AD A046957).

25. Weathersby, P.K., Survanshi, S.S., and Meyer, P. "Reconstruction of 3-D positron emission with maximum likelihood." Naval Medical Research Institute Technical Report No. 88-24, 1988.

Table 1

Characteristics of Data Sets

Data Set	# source locations	Total events	Simulated Gains (ADC units/cm)	Simulated σ (cm)	Simulated f	Simulated offsets
Simulated A	6	1200	3.2	1.25	0	all 0
Simulated B	3	600	3.2	1.25	.143	all 0
Experimental C	15	1596	unknown			
Experimental D	4	881	unknown			

Table 2

Results of fitting to Simulated Data Set A

Simulated with offsets = 0, gains = 3.2, σ = 1.25, f = 0

Model	Offsets	Gain A (unit/cm)	Gain B (unit/cm)	σ (cm)	ⓐ	f	LL
Normal	all < 1	3.26±.02	3.25±.02	1.00±.02	--	--	-1714.8
Huber	all < 1	3.26±.02	3.17±.02	.94±.03	1.500	--	-1733.0
Huber	all < 1	3.24±.02	3.28±.02	1.01±.03	2.9±.9	--	-1714.5
Norm+Uni	all < 1	3.26±.02	3.25±.02	1.00±.02	--	$<10^{-4}$	-1714.8

Table 3

Results of Fitting Models to Simulated Data Set B

Simulated with offsets = 0, gains = 3.2, σ 1.25, f = .14

Model	Offsets (unit)	Gain A (unit/cm)	Gain B (unit/cm)	σ (cm)	(a)	f	LL
Normal	>-22, <65	4.71±.44	6.96±.73	4.79±.27	--	--	-1794.5
Huber	>-10, <22	3.76±.22	4.45±.24	3.20±.13	1.50	--	-1717.8
Huber	>-2.1,<4.4	3.36±.09	3.49±.12	1.08±1.2	.40±.45	--	-1611.6
Norm+Uni	>-.5, <.7	3.25±.04	3.26±.04	1.01±.04	--	.16±.02	-1277.1

Table 4

Results of Fitting Models to Experimental Data Set C

Model	Offsets (unit)	Gain A (unit/cm)	Gain B (unit/cm)	σ (cm)	(a)	f	LL
Normal	>-3.2, <.7	2.36±.05	2.72±.08	5.22±.07	--	--	-4899.5
Huber	>-2.5, <.9	2.21±.04	2.44±.08	3.51±.05	1.50	--	-4636.7
Huber	>-2.7, <1.4	2.21±.04	2.40±.08	2.36±.30	.78±.11	--	-4530.1
Norm+Uni	>-2.5, <1.1	2.18±.03	2.31±.05	2.26±.06	--	.14±.01	-4292.7

Table 5

Results of Fitting Models to Experimental Data Set D

Model	X-ray Offsets (cm)	Gain A (unit/cm)	Gain B (unit/cm)	σ (cm)	ⓐ	f	LL
Normal	3.7±.2, -3.1±.2	1.98±.08	2.40±.11	4.43±.13	--	--	-2559.6
Huber	3.5±.2, -3.4±.2	1.91±.05	2.20±.07	2.94±.06	1.50	--	-2400.5
Huber	3.1±.1, -3.2±.1	1.91±.04	2.12±.06	1.62 .36	.63±.17	--	-2333.6
Normal+uni	3.2±.1, -3.5±.1	1.89±.03	2.11±.05	1.93±.07	--	.13±.01	-2228.0